Optical fiber temperature sensor based on a microcavity with polymer overlay

Iván Hernández-Romano,[1,*] Miguel A. Cruz-Garcia,[2] Carlos Moreno-Hernández,[3] David Monzón-Hernández,[3] Efraín O. López-Figueroa,[4] Omar E. Paredes-Gallardo,[4] Miguel Torres-Cisneros,[5] and Joel Villatoro[6,7]

[1]*CONACYT Research Fellow-Electronics Department, Sede Palo Blanco, University of Guanajuato, Km 3.5 + 1.8, Carr. Salamanca-Valle de Santiago, Salamanca, Guanajuato 36885, Mexico*
[2]*Fiber and Integrated Optics Laboratory, UAM Reynosa-Rodhe, Universidad Autónoma de Tamaulipas, Carr. Reynosa-San Fernando S/N, Reynosa, Tamaulipas 88779, Mexico*
[3]*Centro de Investigaciones en Óptica, Loma del Bosque 115, Colonia Lomas del Campestre, León, Guanajuato 37150, Mexico*
[4]*Departamento de Investigación en Física, División de Ciencias Exactas y Naturales, University of Sonora, Blvd. Luis Encinas y Rosales S/N, Colonia Centro, Hermosillo, Sonora 83000, Mexico*
[5]*Electronics Department, Sede Palo Blanco, University of Guanajuato, Km 3.5 + 1.8, Carr. Salamanca-Valle de Santiago, Salamanca, Guanajuato 36885, Mexico*
[6]*Dept. of Communications Engineering, Escuela Técnica Superior de Ingeniería (ETSI) de Bilbao. University of the Basque Country (UPV/EHU), Alda. Urquijo s/n, E-48013 Bilbao, Spain*
[7]*IKERBASQUE -Basque Foundation for Science, E-48011 Bilbao, Spain*
[*]*heriromano@gmail.com*

Abstract: An ultracompact, cost-effective, and highly accurate fiber optic temperature sensor is proposed and demonstrated. The sensing head consists of Fabry-Perot microcavity formed by an internal mirror made of a thin titanium dioxide (TiO_2) film and a microscopic segment of single-mode fiber covered with Poly(dimethylsiloxane) (PDMS). Due to the high thermo-optic coefficient of PDMS the reflectance of the fiber-PDMS interface varies strongly with temperature which in turn modifies the amplitude of the interference pattern. To quantify the changes of the latter we monitored the visibility of the interference pattern and analyzed it by means of the fast Fourier transform. Our sensor exhibits linear response, high sensitivity, and response time of 14 seconds. We believe that the microscopic dimensions along with the performance of the sensor here presented makes it appealing for sensing temperature in PDMS microfluidic circuits or in biological applications.

OCIS codes: (060.2370) Fiber optics sensors; (120.2230) Fabry-Perot; (130.3990) Micro-optical devices.

References and links

1. D. Janasek, J. Franzke, and A. Manz, "Scaling and the design of miniaturized chemical-analysis systems," Nature **442**(7101), 374–380 (2006).
2. P. Yager, T. Edwards, E. Fu, K. Helton, K. Nelson, M. R. Tam, and B. H. Weigl, "Microfluidic diagnostic technologies for global public health," Nature **442**(7101), 412–418 (2006).
3. H. Craighead, "Future lab-on-a-chip technologies for interrogating individual molecules," Nature **442**(7101), 387–393 (2006).
4. G. M. Whitesides, "The origins and the future of microfluidics," Nature **442**(7101), 368–373 (2006).
5. D. Psaltis, S. R. Quake, and C. Yang, "Developing optofluidic technology through the fusion of microfluidics and optics," Nature **442**(7101), 381–386 (2006).
6. F. Schneider, J. Draheim, R. Kamberger, and U. Wallrabe, "Process and material properties of polydimethylsiloxane (PDMS) for Optical MEMS," Sens. Actuators A Phys. **151**(2), 95–99 (2009).
7. E. Udd, "The Emergence of Fiber Optic Sensor Technology," in *Fiber Optic Sensors: An Introduction for Engineers and Scientists*, 2nd ed., E. Udd, W. B. Spillman, eds. (John Wiley & Sons, 2011).
8. C. L. Lee, J. M. Hsu, J. S. Horng, W. Y. Sung, and C. M. Li, "Microcavity fiber Fabry–Pérot interferometer with an embedded golden thin film," IEEE Photonics Technol. Lett. **25**(9), 833–836 (2013).

#254770 Received 2 Dec 2015; revised 15 Feb 2016; accepted 21 Feb 2016; published 4 Mar 2016

9. B. Sun, Y. Wang, J. Qu, C. Liao, G. Yin, J. He, J. Zhou, J. Tang, S. Liu, Z. Li, and Y. Liu, "Simultaneous measurement of pressure and temperature by employing Fabry-Perot interferometer based on pendant polymer droplet," Opt. Express **23**(3), 1906–1911 (2015).
10. A. Zhou, B. Qin, Z. Zhu, Y. Zhang, Z. Liu, J. Yang, and L. Yuan, "Hybrid structured fiber-optic Fabry-Perot interferometer for simultaneous measurement of strain and temperature," Opt. Lett. **39**(18), 5267–5270 (2014).
11. H. Y. Choi, K. S. Park, S. J. Park, U. C. Paek, B. H. Lee, and E. S. Choi, "Miniature fiber-optic high temperature sensor based on a hybrid structured Fabry-Perot interferometer," Opt. Lett. **33**(21), 2455–2457 (2008).
12. Z. L. Ran, Y. J. Rao, W. J. Liu, X. Liao, and K. S. Chiang, "Laser-micromachined Fabry-Perot optical fiber tip sensor for high-resolution temperature-independent measurement of refractive index," Opt. Express **16**(3), 2252–2263 (2008).
13. C. L. Lee, L. H. Lee, H. E. Hwang, and J. M. Hsu, "Highly sensitive air-gap fiber Fabry–Pérot interferometers based on polymer-filled hollow core fibers," IEEE Photonics Technol. Lett. **24**(2), 149–151 (2012).
14. X. L. Tan, Y. F. Geng, X. J. Li, Y. L. Deng, Z. Yin, and R. Gao, "UV-Curable Polymer Microhemisphere-Based Fiber-Optic Fabry–Perot Interferometer for Simultaneous Measurement of Refractive Index and Temperature," IEEE Photonics J. **6**(4), 1–8 (2014).
15. X. Y. Zhang, Y. S. Yu, C. C. Zhu, C. Chen, R. Yang, Y. Xue, Q. D. Chen, and H. B. Sun, "Miniature end-capped fiber sensor for refractive index and temperature measurement," IEEE Photonics Technol. Lett. **26**(1), 7–10 (2014).
16. C. Moreno-Hernández, D. Monzón-Hernández, I. Hernández-Romano, and J. Villatoro, "Single tapered fiber tip for simultaneous measurements of thickness, refractive index and distance to a sample," Opt. Express **23**(17), 22141–22148 (2015).
17. R. Mukhopadhyay, "When PDMS isn't the best. What are its weaknesses, and which other polymers can researchers add to their toolboxes?" Anal. Chem. **79**(9), 3248–3253 (2007).
18. I. Martincek, D. Pudis, and P. Gaso, "Fabrication and optical characterization of strain variable PDMS biconical optical fiber taper," IEEE Photonics Technol. Lett. **25**(21), 2066–2069 (2013).
19. A. L. Thangawng, R. S. Ruoff, M. A. Swartz, and M. R. Glucksberg, "An ultra-thin PDMS membrane as a bio/micro-nano interface: fabrication and characterization," Biomed. Microdevices **9**(4), 587–595 (2007).
20. D. Fuard, T. Tzvetkova-Chevolleau, S. Decossas, P. Tracqui, and P. Schiavone, "Optimization of poly-di-methyl-siloxane (PDMS) substrates for studying cellular adhesion and motility," Microelectron. Eng. **85**(5-6), 1289–1293 (2008).
21. S. L. Peterson, A. McDonald, P. L. Gourley, and D. Y. Sasaki, "Poly(dimethylsiloxane) thin films as biocompatible coatings for microfluidic devices: cell culture and flow studies with glial cells," J. Biomed. Mater. Res. A **72**(1), 10–18 (2005).
22. R. Seemann, M. Brinkmann, T. Pfohl, and S. Herminghaus, "Droplet based microfluidics," Rep. Prog. Phys. **75**(1), 016601 (2012).
23. C. E. Lee, H. F. Taylor, A. M. Markus, and E. Udd, "Optical-fiber Fabry-Perot embedded sensor," Opt. Lett. **14**(21), 1225–1227 (1989).
24. Y. H. Kim, K. S. Park, B. H. Lee, S. Lee, D. H. Woo, and Y. T. Chough, "Highly accurate refractive index sensor based on Fourier-transformed phase acquisition in fiber-optic interferometer," in Proceeding of International Conference In Sensing Technology, (IEEE, 2013) pp. 555–558.
25. J. Villatoro, V. P. Minkovich, and J. Zubia, "Photonic crystal fiber interferometric force sensor," IEEE Photonics Technol. Lett. **27**(11), 1181–1184 (2015).
26. D. Barrera, V. Finazzi, J. Villatoro, S. Sales, and V. Pruneri, "Packaged optical sensors based on regenerated fiber Bragg gratings for high temperature applications," IEEE Sens. J. **12**(1), 107–112 (2012).

1. Introduction

In the last twenty years lab on a chip (LOC) devices have emerged as a feasible technology for a number of applications such as analytical chemistry [1], point-of-care diagnostics [2], genomic research [3], etc. One of the most promising LOC devices addresses the integration of microfluidics [4] technology and optical interrogation techniques. The popular material to fabricate such optofluidic devices is PDMS (Polydimethylsiloxane) [5,6] since it is biocompatible, nontoxic, optically transparent, inexpensive, and easy to fabricate in not controlled nor specialized facilities. In these devices the presence of the targeted agent involves a change in the refractive index (RI) of the fluid. Different approaches to measure the tiny RI changes associated to biological reactions have been successfully demonstrated in controlled lab conditions [5]. Especial attention has been paid to temperature stability since it is well known that RI of most polymers varies with temperature. However, in real world applications where temperature is difficult to control, one option is to measure RI and temperature simultaneously. In this sense an alternative is the integration of a temperature sensor in the PDMS microfluidic circuit. To this end, optical fiber sensors are good candidates

#254770 Received 2 Dec 2015; revised 15 Feb 2016; accepted 21 Feb 2016; published 4 Mar 2016

since they are lightweight and compact, biocompatible, chemically inert, can be easily integrated in a telecommunication network for remote and real-time sensing [7].

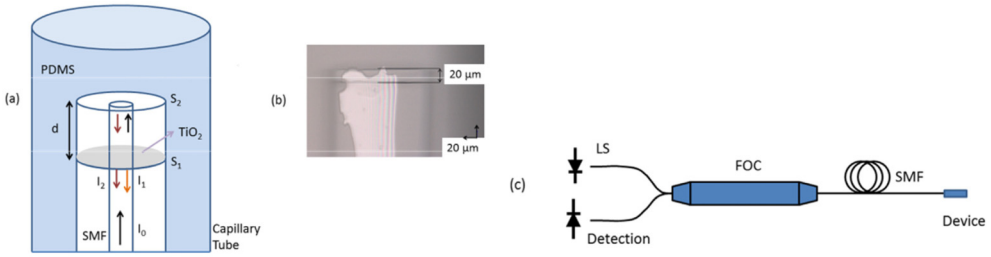

Fig. 1. (a) Schematic diagram of the sensing head, S_1 provides the reference beam and S_2 the probe beam. (b) Image of the cavity composed by an internal mirror and the cleaved end of a SMF. (c) The interrogation of the device involves a light source (LS), a fiber optic circulator (FOC) or coupler and a power meter (PM).

Fiber sensors in a Fabry-Perot configuration are the simplest and easiest to fabricate [7]. A number of fiber Fabry-Perot interferometers have been studied and fabricated due to their capability of measuring physical quantities such as refractive index (RI) [8], pressure [9], strain [10], and temperature [9]. The implementation of Fabry-Perot cavities (FPCs) on the tip of an optical fiber, for sensing temperature for example, is appealing since they combine low-cost fabrication, microscopic size and high sensitivity. Among the techniques used to build compact cavities (~100 μm) we can mention thin films embedded in single mode fiber (SMF) [9], hollow core fiber spliced to SMF [11], femtosecond laser micromachining [12], polymer cavities formed by dip coating [9, 13–15]. In the majority of such interferometers the thermo-optic properties of the cavity is exploited. Therefore, in such sensors, temperature induces a shift of the interference pattern. Since the thermo-optic coefficient (TOC) of is small ($6.3\text{x}10^{-6}$/°C) [12], thus, in most FPCs a large temperature change is needed to produce a measurable interference pattern shift. The low thermal sensitivity is a disadvantage for measuring temperature changes in the range between 20 to 60 °C which is the range of interest for biological applications or in LOC devices. To overcome this limitation, FPCs made of polymer with a high TOC that exhibit high sensitivities in the aforementioned temperature range have been fabricated [9, 13–15]. Three commercial polymers have been used for this purpose, PDMS, NOA61, and NOA65 whose TOCs are $-4.66\text{x}10^{-4}$/°C [16], $-1.17\text{x}10^{-4}$/°C [14], and $-1.83\text{x}10^{-4}$/°C [9], respectively. One drawback of temperature sensors reported in [9, 13–15] is that they need to be calibrated when a physical variable, for example RI or pressure.

In this work, we propose and demonstrate a simple, cost-effective, and highly accurate temperature sensor based on a single mode fiber FPC covered with PDMS, see Fig. 1(a). The interferometer was built by depositing a 169 nm-thick film of TiO_2 over the cleaved face of a standard SMF. The TiO_2 coated fiber was then fusion spliced to another SMF which was cleaved at a distance of 20 or 230 μm from the TiO_2 film. The cleaved face of the SMF was in direct contact with PDMS. To do so, the device was placed inside a capillary tube filled with PDMS. In our configuration, the mirrors of the cavity are the TiO_2 film and the cleaved SMF-PDMS interface, see Fig. 1(a).

In our device, temperature alters the RI of PDMS, and thereby, the reflectance of the interface between fiber core and the PDMS. As a consequence, the amplitude of the interference pattern is changed. To quantify the changes in amplitude of the interference pattern two signal processing techniques were used. In one of them the extinction ratio (ER), i.e., the difference between maxima and minima of the interference fringes, was monitored. In the other case the peak amplitude of the Fast-Fourier-Transform (FFT) of the interference pattern was monitored. The latter technique was used to demonstrate the real-time

#254770 Received 2 Dec 2015; revised 15 Feb 2016; accepted 21 Feb 2016; published 4 Mar 2016

temperature measurement capabilities of our device. We chose PDMS polymer for building our sensor because it is nontoxic [17], it has low absorption at 1550 nm [18], and it is biocompatible [19]. Due to its biocompatibility, it has been employed for cell-based studies [20] and tissue engineering [21]. Additionally, PDMS is the most commonly used material in the standard microfluidics devices [22].

2. Design and principle

The proposed device is shown in Fig. 1(a). To fabricate a Fabry-Perot microcavity in SMF we first coated the cleaved end of the SMF with a dielectric material (TiO_2 in our case). The evaporation of TiO_2 was carried out in a high vacuum chamber. The thickness of the film was was 169 nm, it was measured with a crystal quartz monitor. We chose TiO_2 as it has good stability and high mechanical strength; moreover, it can withstand the elevated temperature during the fusion splicing of the optical fibers [23]. The dielectric film on the SMF works as a partially reflecting internal mirror and provides the reference beam for the Fabry-Perot interferometer. Then, the TiO_2-coated fiber was fusion spliced to a segment of SMF which was cleaved from distance of 20 or 238 μm from the dielectric mirror, see Fig. 1(b). The interface between the cleaved SMF end and air (or a polymer) provides the probe or sensing beam. The recombination between the reference and probe beams is what produces an interference pattern. It is interesting to note that the excitation and recombination of the beams is carried out inside a conventional optical fiber.

The reflectance of the TiO_2 film was measured by launching light (wavelength 1550 nm) from a highly stable tunable laser to the coated fiber end through an optical circulator, see Fig. 1(c). The reflected light was detected by a power meter. Without any deposited film the reflectance at the interface between the fiber core and air was −14.81 dB. However, when the cleaved SMF end was coated with a 169 nm-thick TiO_2 film the reflectance reached −7.87 dB. As it is know that the reflectance of a TiO_2 film decreases drastically after a fusion splicing process, several tests were carried out until we achieved an internal mirror (TiO_2-coated SMF fusion splicing to and non-coated SMF) with reflectance of −36.58 dB which is higher than the reflectance of the interface formed by the fiber core and PDMS polymer (−40.46 dB, at 24 °C). The next step in the fabrication of the microcavity involves a cleaving process under an optical microscope. The cavity had a length of 20 or 238 μm, although other lengths are possible as the cavity length does not affect the performance of our temperature sensor as we will see later on.

It is convenient to point out that in a thin film evaporation chamber hundred of cleaved SMFs can be coated in the same evaporation process. In addition, state-of-the-art fusion splicing machines allow developing ad hoc or optimized splicing and cleaving programs which ensures reproducibility and low fabrication cost. The final step in the fabrication of the sensor involves coating a surface of the FP cavity with a thermo-optic material. To do so, the fiber tip was placed inside a capillary tube whose inner diameter, wall thickness, and length were 1.1 mm, 0.2 mm, and 13 mm, respectively. The tube was filled with PDMS by capillary action. PDMS polymer was cured following the curing process provided by the manufacturer. The interface between the PDMS polymer and the cleaved SMF face provides the temperature-sensitive beam.

The behavior of the device shown in Fig. 1(a) can be explained as follows. Light reflects from two interfaces, denoted as S_1 (TiO_2 film) and S_2 (interface between fiber core and PDMS). If light with intensity I_0 is launched into the fiber, then the surface S_1 will reflect part of the light and the rest will be transmitted. The intensity of the reflected light from S_1 is denoted as I_1. Similar effect occurs at the surface S_2. The reflected intensity from the surface S_2 is denoted by I_2. The intensities I_1 and I_2 are collected and combined by the SMF core. As the reflectance of the surfaces S_1 and S_2 is low, multiple reflections can be neglected. Therefore, our device can be treated as a two beam interferometer. The intensities I_1 and I_2

#254770 Received 2 Dec 2015; revised 15 Feb 2016; accepted 21 Feb 2016; published 4 Mar 2016

can be written as $I_1 = I_0 R_1$ and $I_2 = (1-A)^2 (1-R_1)^2 R_2 I_0$, respectively, where A is the transmission loss factor of the surface S_1. R_1 and R_2 are the reflectivities of the surfaces S_1 and S_2, respectively. The intensity I_R of the light reflected from the cavity that will reach the power meter can be expressed by [5]

$$I_R = R_1 I_0 + (1-A)^2 (1-R_1)^2 R_2 I_0 + 2(1-A)(1-R_1)\sqrt{R_1 R_2} I_0 \cos(\varphi) \qquad (1)$$

where $\varphi = 4\pi n_{eff} d/\lambda$ is the phase difference between the reference and the sensing beams. n_{eff} is the effective refractive index of the fundamental mode propagating in the SMF core, d is the cavity length, and λ is the wavelength of the optical source. Therefore, if one launches light from a broadband source to the device and analyzes the reflected spectrum a sinusoidal (interference) pattern can be expected.

Our device is highly sensitive to temperature because the PDMS polymer has a high TOC. A minute variation in temperature will modify the polymer refractive index, and consequently, the reflectance of the surface S_2, this means R_2. As a result, the maxima and minima of the interference pattern will change. Temperature will also alter n_{eff} and d, hence φ, giving rise to a shift of the interference pattern. The optical fiber has a low TOC ($6.3\text{x}10^{-6}$/°C) [12], and a low thermal expansion coefficient ($0.55\text{x}10^{-6}$/°C) [12]. Therefore, the shift of the interference pattern will be minimal for a small temperature change. In our case, we do not monitor the shift of the interference pattern but the changes of the visibility or fringe contrast (difference between maxima and minima of the interference pattern). To predict such changes we used the Sellmeier equation [6], the TOC [16] for the PDMS, and the equation $R_2 = \left[(n_{eff} - n_{PDMS}) / (n_{eff} + n_{PDMS}) \right]^2$, where n_{PDMS} is the RI of the PDMS and $n_{eff} = 1.44630$. Figure 2(a) shows the interference patterns at temperature between 22 to 60 °C. In such temperature range the the RI of PDMS goes from 1.42039 to 1.40268.

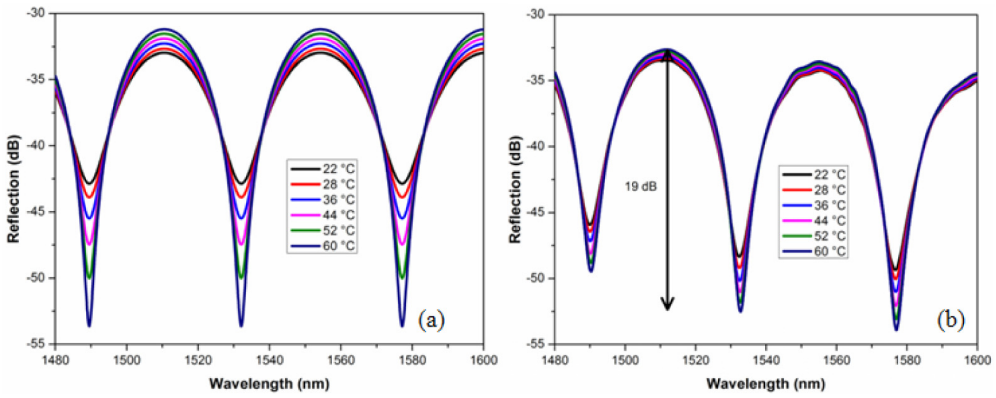

Fig. 2. (a) Simulation of the reflection spectra of the device shown in Fig. 1(a) at difference temperatures. (b) Interference patterns observed in a 20 μm-long Fabry-Perot cavity in PDMS at different temperatures

3. Results and discusison

The experimental setup that was used for testing the proposed devices is shown in Fig. 1(c). Light from a Super-Luminescent Light Emitting Diode (SLED), center at 1550 nm, was launched to the cavity by means of a fiber optic circulator. The reflected light was detected by an optical spectrum analyzer (OSA). The sensor was placed on a thermoelectric cooler, inside a closed box, and the temperature was increased from 22 °C to 60 °C. Figure 2(b) shows the spectra observed at different temperatures. The extinction ratio (ER) of the interference patterns was correlated with temperature [15]. The ER can be calculated by using Eq. (1) as follows,

#254770 Received 2 Dec 2015; revised 15 Feb 2016; accepted 21 Feb 2016; published 4 Mar 2016

$$ER = 10\log_{10}\left[\frac{R_1 + (1-A)^2 (1-R_1)^2 R_2 + 2(1-A)(1-R_1)\sqrt{R_1 R_2}}{R_1 + (1-A)^2 (1-R_1)^2 R_2 - 2(1-A)(1-R_1)\sqrt{R_1 R_2}}\right] \quad (2)$$

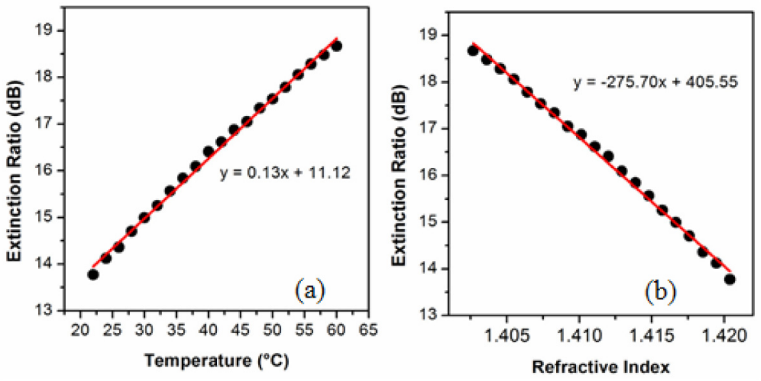

Fig. 3. (a) Variation of the ER at different temperatures. (b) Variation of the ER at different RIs of the PDMS. The dots are experimental values and the solids lines fitting lines to the experimental data. The length of the cavity was 20 μm.

The observed variation of the ER as a function of temperature is shown in Fig. 3(a). The corresponding variation of the ER as a function of the RI of the PDMS is shown in Fig. 3(b). The temperature sensitivity was found to be 0.13 dB/°C.

The method described above suggests a high temperature sensitivity of our device, however, the monitoring of ER is not very accurate because it depends on which peaks and dips are selected. A more accurate method is by analysing the interference patterns by means of the Fast Fourier Transform (FFT) as this provides information of the phase [24], frequency [11] and amplitude [25] of such patterns. It has been shown that the FFT method provides higher resolution [24]. Figure 4(a) was obtained by applying the FFT to the fringe interference patterns shown in Fig. 2(b). The normalized FFT peak as a function of temperature is shown in Fig. 4(b). In order to show that the cavity length is not an issue a large cavity was constructed (238 μm, reflectance of the internal mirror −37.16 dB), following the fabrication steps mention above, and it was also analyzed by the FFT method. The calculated FFT of the spectra and the normalized amplitudes of the FFT peaks as function of temperature are shown in Figs. 4(c) and in (d), respectively. By comparing the Figs. 4(a) and (c), one can observed that the FFT peak of Fig. 4(c), i.e., of the longer device, is sharper that the peak shown in Fig. 4(a), or shorter device. Since the spectra of the larger cavity have more periods, the shape of the FFT is smoother which is easier to track. It can be noted from Figs. 4(b) and 4(d) that the behavior of our devices is linear.

An important parameter of any temperature sensor is its response time. In our case we define it as the time required for our sensor output to go from 10% to 90% of the maximum amplitude change. To measure such a time a simple experimental setup was implemented; it

#254770 Received 2 Dec 2015; revised 15 Feb 2016; accepted 21 Feb 2016; published 4 Mar 2016

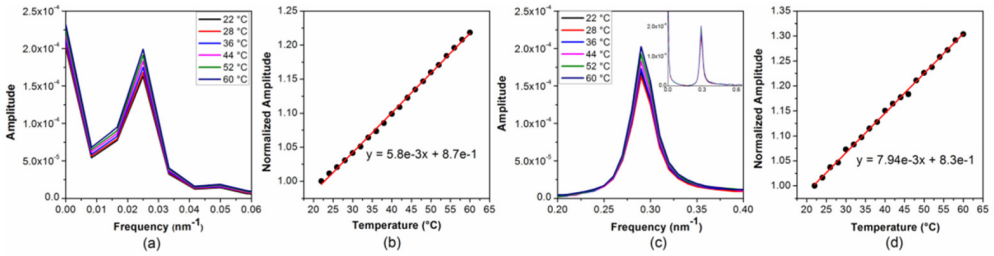

Fig. 4. Cavity length 20 μm: (a) Calculated FFT of the spectra shown in Fig. 3, (b) Normalized amplitude of the FFT peak as a function of temperature; Cavity length 238 μm: (c) Calculated FFT of the spectra, the inset shows higher span, (d) Normalized amplitude of the FFT peak as a function of temperature.

consisted of a personal computer, a spectral interrogator, and the sensor device mounted in a translation stage. The spectral interrogator (sm125, Micron Optics), which had a tunable laser emitting from 1510 to 1590 nm with a 20 Hz repetition rate, was connected to the sensor with a sampling rate of 1 sample/s. A program in LabView was developed to acquire the peak amplitude of the FFT and to store it in personal computer. A more detailed description of this scheme can be found elsewhere [16]. In order to determine the heating up and the cooling down response time of our sensor an automatic system with translations stages was developed. Such system held the sensor in the air, for 5 min, at room temperature (26 °C) and then it was dipped into a container with water at 60 °C for another 5 min. Such process was repeated several times. Figure 5 shows the peak amplitude of the FFT for the two temperatures mentioned above as a function of time. The oscillations observed in the FFT peak are due oscillations in temperature of the hot water because it was heated with a hotplate. It is worth noting that the sensor is capable of following the small temperature variations of the hotplate we used. The heating up and the cooling down response time were found to be 14 s and 31 s, respectively. These times are comparable to those of a sensor based on a fiber Bragg grating reported by D. Barrera et al. [26].

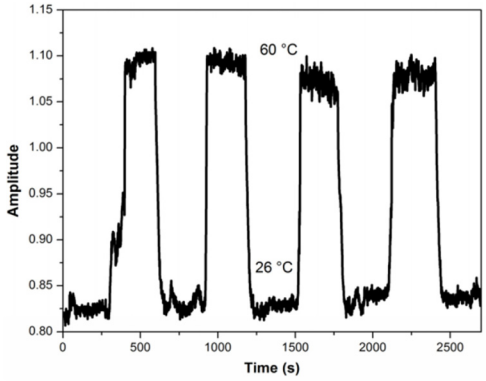

Fig. 5. Temperature cycling test to determine the response time of the proposed devices. The length of the cavity was 20 μm.

4. Conclusions

In conclusion, we have proposed and demonstrated an ultracompact, simple-to-fabricate, and highly accurate temperature sensor based on a single mode fiber Fabry-Perot cavity embedded in PDMS polymer. In our device, the maxima and minima of the reflected interference spectrum depend on the RI of the PDMS which has a high thermo-optic coefficient. Small variations in temperature (in the 22 to 60 °C range) can cause a detectable change in the

#254770 Received 2 Dec 2015; revised 15 Feb 2016; accepted 21 Feb 2016; published 4 Mar 2016

interference pattern. By monitoring the extinction ratio of the interference pattern a temperature sensitivity of 0.13 dB/°C was observed. Two FPCs with different lengths were constructed and tested by the fast Fourier transform technique and similar results were obtained. In this case, temperature is codified in the FFT peak which can be monitored easily. The interrogation of our device is simple as an LED and a low-resolution spectrum analyzer can be used. In addition, the materials, components, and tools needed to fabricate the device are widely available. Due to the extensive use of PDMS in biological and microchannel applications we believe that our microscopic device can be employed for monitoring the temperature in those structures. In fact, the fiber tip can be inserted in the PDMS substrate or mold during the fabrication process to sense temperature or refractive index.

Acknowledgments

I. Hernández-Romano and M. Torres-Cisneros acknowledge the funding through the project: "Cátedras CONACYT 2015", "Cátedras de excelencia Universidad de Guanajuato 2014" and "Convocatoría CIO-UG 2015". J. Villatoro is grateful to the Ministerio de Economía y Competitividad (Spain) for financial support under project TEC2015-63826-C3-1.

#254770 Received 2 Dec 2015; revised 15 Feb 2016; accepted 21 Feb 2016; published 4 Mar 2016